Abnormal volumetric thermal expansion in the hourglass fermion materials KHgAs and KHgSb

Dahu Chang,[1,2] Chun-Yao Niu,[1,*] Xiaowei Huang,[3] Qiang Sun,[1] Jun-Hyung Cho,[4,1] and Yu Jia[1,3,*]

[1]*International Laboratory for Quantum Functional Materials of Henan, and School of Physics and Engineering, Zhengzhou University, Zhengzhou 450001, China*

[2]*Department of Mathematics and Physics, Luoyang Institute of Science and Technology, Luoyang 471023, China*

[3]*Key Laboratory for Special Functional Materials of Ministry of Education, and School of Physics and Electronics, Henan University, Kaifeng 475001, China*

[4]*Department of Physics and Research Institute for Natural Sciences, Hanyang University, 17 Haengdang-Dong, Seongdong-Ku, Seoul 133-791, Korea*

(Received 4 December 2016; revised manuscript received 24 January 2017; published 8 March 2017)

Using first principles density functional theory calculations combined with quasi-harmonic approximation, we demonstrate that the recently reported nonsymmorphic "hourglass fermion" materials KHgX (X = As, Sb) belong to a type of negative thermal expansion (NTE) material with an abnormal volumetric thermal expansion. It is revealed that the NTE is caused by the peculiar layered structures of KHgAs and KHgSb, composed of alternately arranged alkali metal and Hg-X atomic layers with residual tensions. Specifically, the coefficients of negative thermal expansion (CNTE) of KHgAs and KHgSb can reach up to $-2.7 \times 10^{-6}\,\mathrm{K}^{-1}$ and $-4.9 \times 10^{-6}\,\mathrm{K}^{-1}$ along the a axis, respectively, as well as a larger volumetric CNTE of $-4.98 \times 10^{-6}\,\mathrm{K}^{-1}$ for KHgSb. The analyses of Grüneisen parameters and vibrational modes show that the NTE of KHgX is driven by the cooperation of membrane and tension effects. It is most likely that the weaker bonds in the Hg-X layer and the smaller mass of alkali metal facilitate the membrane and tension effects, therefore producing a large NTE. Our findings offer insights for understanding the underlying mechanism of NTE behavior in the hourglass fermion materials KHgX.

DOI: 10.1103/PhysRevB.95.104101

I. INTRODUCTION

Nontrivial topological quantum materials (TQMs), such as topological insulators (TIs), Dirac semimetals (DSMs), and Weyl semimetals (WSMs) [1–6], have raised great interest in condensed matter physics. At the same time, many efforts have been made to discover new types of fermions. Very recently, *ab initio* calculations of Wang *et al.* [7,8] predicted the so-called "hourglass fermion" materials with nonsymmorphic structure and the hourglass-shaped dispersion relation; subsequently, an angle-resolved photoemission spectroscopy experiment [9] confirmed their electronic properties. As the first family of hourglass fermion materials, KHgX (X = As, Sb) have various electronic properties, such as topological insulators, hourglass-shaped electronic channels, and three-dimensional doubled quantum spin Hall effects [7]. Therefore, these topological materials may be utilized in the application of efficient transistor switching in the future.

For practical reasons, the thermal properties of hourglass fermion materials, such as thermal conductivity and thermal expansion, have to be understood for their efficient utilization in electronic device applications. As one of the important thermal properties, negative thermal expansion (NTE) behavior has attracted much attention [10] since the discovery of the abnormal behavior of ZrW_2O_8 in 1996 [11]. It is well known that NTE behavior is determined by many factors, such as phonon vibration [12–14], charge transfer [15], and magnetic phase transition [16,17]. Specifically, the NTE materials caused by the vibrational effects have not only the open framework structures [18–20], but also the relatively rare layered structures [e.g., graphite, $Ni(CN)_2$ and $CuNi(CN)_4$] [21–23]. The vibrational effects, including the transverse vibration of bridge atom and the rigid unit modes (RUMs), can be more dominant in the open framework structure. For the layered structures, Lifshitz predicted the "membrane effect" or "bending effect" to explain the NTE mechanism [24]. Besides the membrane effect, the tension effects of optical modes may also contribute to the NTE of layered compounds. It should be noted that, in the layered compounds mentioned above, NTE behaviors are only limited in the layer plane, while the volume exhibits positive thermal expansion. Such a picture in the layered compound seems to work well so far, without exception.

The structure of hourglass Fermion materials KHgX is composed of alternately alkali-metal K and honeycomb Hg-X atomic layers (see Fig. 1). Here, the Hg-X atomic layers constitute the main skeleton of KHgX, which is stabilized by the alkali-metal atomic layer. This peculiar layered structure of KHgX may be associated with their NTE properties, which would be of interest, together with their topological and superconductive properties. However, the thermodynamic properties of KHgX have not been explored so far, especially for their NTE properties. In this paper, we investigate the vibrational and NTE properties of KHgX (X = As, Sb) by using first principles density functional theory (DFT) calculations combined with quasi-harmonic approximation. We find that both KHgAs and KHgSb exhibit NTE within the layer plane as well as over the volume due to their peculiar structures, which can be regarded as a type of NTE material. The analyses of Grüneisen parameters and vibrational modes reveal that the NTE of KHgX is driven by the cooperation of membrane and tension effects. It is thus demonstrated that the weaker bonds in Hg-X and the relatively smaller mass of the alkali metal can facilitate the membrane and tension

*Corresponding authors: niuchunyao@zzu.edu.cn; jiayu@zzu.edu.cn

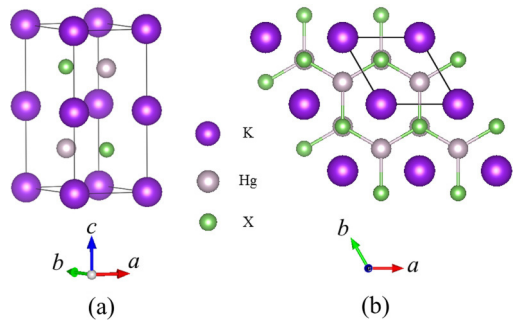

FIG. 1. Crystal structure of KHgX (X = As, Sb): (a) side (b) top views.

effects, giving rise to a large NTE. The present findings have implications for understanding the underlying mechanism involved in the NTE properties of KHgX.

II. COMPUTATIONAL METHOD

Our first principles DFT calculations were performed using the Vienna *Ab initio* Simulation Package (VASP) [25] with the projector augmented wave (PAW) method [26]. For the treatment of exchange-correlation energy, we employed the generalized gradient approximation (GGA) functional of Perdew-Burke-Ernzerhof (PBE) [27]. Here, the PAW projection was performed in reciprocal space. The precision of the charge density grid was set automatically so as to avoid aliasing errors, and an additional support grid containing eight times the number of points was used to evaluate the augmentation charges. The VASP pseudopotentials were generated by modeling valence electrons $3s^2\,3p^6\,4s^1$ for K, $5d^{10}\,6s^2$ for Hg, $4s^2\,4p^3$ for As, and $5s^2\,5p^3$ for Sb. The kinetic energy cutoff of the plane wave basis set was taken to be 500 eV, and the $\boldsymbol{k}$-space integration was done with the Monkhorst-Pack meshes of $(16\times16\times8)$. Convergence criteria for the electronic and the ionic relaxation were an energy of 10^{-8} eV and a force of 10 eV/Å, respectively. Vibrational properties were calculated through the Phonopy code [28], while the real space force constants were calculated in the density functional perturbation theory (DFPT) as implemented in VASP. The thermal expansion calculations are based on the quasi-harmonic approximation (QHA), where the Helmholtz free energy is given by [29]

$$F(V,T) = E(V) + k_B T \sum_{v,q} \log\left\{2\sinh\left(\frac{\hbar\omega_v(q,V)}{2k_B T}\right)\right\}. \tag{1}$$

Here, $E(V)$ is the ground-state energy obtained using the DFT, and the second term is the vibrational contribution to the free energy, where $\omega_v(q,V)$ is the phonon frequency at a fixed volume V and a given wave vector q. To obtain the volume at a given temperature, we choose 16 different volumes near the optimized equilibrium position [ranging $\Delta a/a(\Delta c/c) = \pm2.4\%$] to fit the isothermal F-V curves by using the Murnaghan equation of state (EOS) [30]. For the QHA calculations, we employed a supercell of the $3\times3\times2$ unit cell. Finally, the coefficient of thermal expansion (CTE) within QHA can be determined [31] by

$$\alpha_V(T) = \frac{1}{BV}\sum_i \gamma_i(T) C_{V_i}(T). \tag{2}$$

TABLE I. Calculated lattice constants a and c (Å) and bulk modulus B (GPa) of KHgX compared with those of the experiment (Expt.) in Ref. [32].

	KHgAs		KHgSb	
	Calc.	Expt. [32]	Calc.	Expt. [32]
a	4.622	4.506	4.898	4.784
c	10.250	9.976	10.523	10.225
B	28.96		24.46	

Here B, $\gamma_i(T)$ and $C_{V_i}(T)$ are the bulk modulus, Grüneisen parameter, and specific heat capacity of the ith vibration state at a given temperature, respectively.

III. RESULTS AND DISCUSSION

A. Phonon spectrum and thermal vibrational property

We begin to consider the geometries of KHgAs and KHgSb. As shown in Fig. 1, KHgX (X = As, Sb) crystals consist of the honeycomb layers of Hg and As/Sb atoms, with AB stacking along the c axis, between which a triangular lattice of K atoms exists; the K atoms are located on top of the center of the honeycomb lattice, while the As/Sb/Hg atoms are located on top of the center of the triangular lattice. The nonsymmorphic space group is $D^4_{6h}(P6_3/mmc)$, and the crystallographic unit cell contains two formula units. The K, Hg, and As/Sb atoms are positioned at 2a (0, 0, 0), 2c (1/3, 2/3, 1/4), and 2d (1/3, 2/3, 3/4) Wyckoff sites, respectively.

To obtain the equilibrium structures of KHgX, we calculate the total energies as a function of volume. Using the Murnaghan EOS, we find the equilibrium lattice constants ($a = b, c$) and bulk modulus, which are listed in Table I. Our calculated lattice constants a and c are found to be in reasonable agreement with the experimental data [32]. However, the slightly overestimated PBE lattice constants compared with experimental values may in turn give rise to the underestimations of bulk modulus, as well as the size of the NTE effect [33], as discussed below.

Since the bulk modulus reflects the measure of resistance to compressive deformation within the limits of the elastic regime, a smaller bulk modulus in the layered materials is likely related to the NTE. Indeed, Table I shows that the calculated bulk moduli of KHgAs and KHgSb are 28.96 and 24.46 GPa, respectively, which are relatively smaller than the isostructural low-temperature superconductor SrPtAs (66.1 GPa) [34], layered NTE graphite materials (35.8 GPa) [21], and $Ni(CN)_2$ (63.4 GPa) [22]. We note that the bulk modulus is effectively an average of elastic constants along the crystallographic axes. The full elastic-constant matrices of KHgAs and KHgSb are given in Table S2 of the Supplemental Material [35].

To examine the possibility of the NTE of KHgX, we calculate their phonon dispersion curves and the phonon density of states (DOS). The results are given in Fig. 2. We find that the phonon dispersion curves of KHgX have no imaginary frequencies along high-symmetry directions in the Brillion zone (BZ), indicating that their structures are dynamically stable. We note that the phonon dispersions of KHgAs and

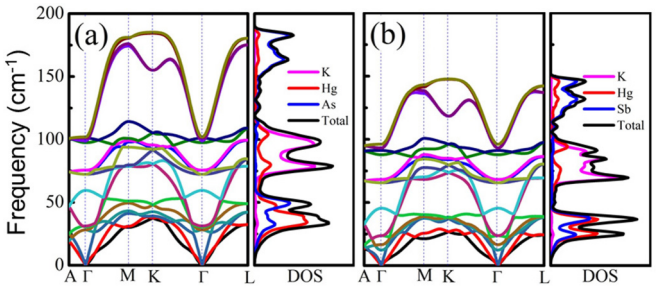

FIG. 2. Calculated phonon dispersion curves and phonon DOS of (a) KHgAs and (b) KHgSb.

KHgSb are similar to each other because of their similar geometries. It is noticeable that, when As atoms are substituted by Sb atoms in KHgX, the vibrational energy range is found to decrease drastically. From the calculated phonon DOS, it is seen that the vibration frequency can be split into three regions: the low-frequency phonon modes mainly arise from the vibrations between Hg and X, while the medium- and high-frequency phonon modes are due to the vibrations of K and X atoms, respectively. Since NTE mostly originates from the low-frequency vibration modes, it is likely that the cooperative vibrations of Hg and X would contribute to the NTE of KHgX.

Since the primitive cell of KHgX contains six atoms, there are 18 normal modes, including three acoustic and 15 optical modes. Using point group analysis [34], the zone-center optical modes (at the Γ point) of hexagonal KHgX can be classified as $2A_u + 2B_{2g} + B_{1u} + 2E_{2g} + 2E_{1u} + E_{2u}$. Here, two A_u and two E_{1u} modes are infrared active, two E_{2g} modes are Raman active, and the remaining modes are optically silent. The calculated zone-center optical phonon frequencies of KHgAs and KHgSb with respect to the mode representation are listed in Table II. The vibration diagram corresponding to the zone-center optical phonon modes of KHgX is given in Fig. 3. Based on these data, we find that the lower energy modes of $E_{2g}(1)$, $B_{2g}(1)$, A_{2u}, and E_{2u} are only associated with the vibrations of the honeycomb layer atoms, while the other modes are due to the vibrations of the alkali-metal layer atoms. Specifically, the modes of $B_{2g}(1)$, A_{2u}, and E_{2u} are the vibrations of Hg and/or Sb perpendicular to the honeycomb plane, which mostly contribute to the NTE of KHgX as discussed below.

TABLE II. Calculated zone-center optical phonon frequencies (cm^{-1}) of KHgX (X = As, Sb).

Modes	KHgAs	KHgSb
$E_{2g}(1)$	28.15	12.33
$B_{2g}(1)$	30.54	16.54
A_{2u}	31.25	23.69
E_{2u}	59.55	45.57
$E_{1u}(1)$	72.29	65.57
$B_{2g}(2)$	75.58	68.18
B_{1u}	97.45	87.78
A_{1u}	98.94	91.17
$E_{2g}(2)$	101.00	93.11
$E_{1u}(2)$	102.00	96.11

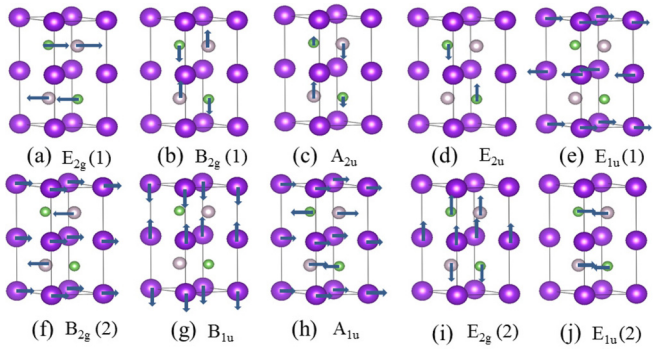

FIG. 3. Schematic diagram of the eigenvector representations for the zone-center optical phonon modes of KHgX.

B. Negative thermal expansion property

Our DFT calculations within the QHA obtain the CTEs for KHgAs and KHgSb with respect to volume as well as along the a and c axes, as shown in Figs. 4(a) and 4(b), respectively. Here, volume relaxations are performed at the QHA-predicted lattice volumes for a range of temperatures in order to estimate the temperature dependence of a and c lattice parameters. We find three main features for the NTE properties of these KHgX layered materials. First, both KHgAs and KHgSb exhibit NTE behaviors within the ab plane at temperatures below ~40 K, and the maximal negative CTE along the a axis amounts to about -2.7×10^{-6} K^{-1} and -4.9×10^{-6} K^{-1} for KHgAs and KHgSb, respectively. The NTE of KHgSb in the ab plane is almost four times larger (-1.2×10^{-6} K^{-1}) than that of graphite, thereby being regarded as a layered material with a significant NTE value. We note that the most layered materials, such as bulk BN, black and blue P, MoS_2, and $MoTe_2$, do not exhibit NTE behavior. Meanwhile, a few layered materials, such as graphite and $Ni(CN)_2$, have NTE in the honeycomb layer, but they have a volumetric positive thermal expansion (PTE). Intriguingly, KHgSb exhibits a large volumetric NTE property (below ~25 K) with a significant negative CTE of about -4.98×10^{-6} K^{-1} at 15 K [see Fig. 4(b)], which is almost half the value of the star material ZrW_2O_8. To the best of our knowledge, KHgSb is the first layered material with a large volumetric NTE property. This presence of the volumetric NTE in KHgSb may be due to a relatively greater NTE in

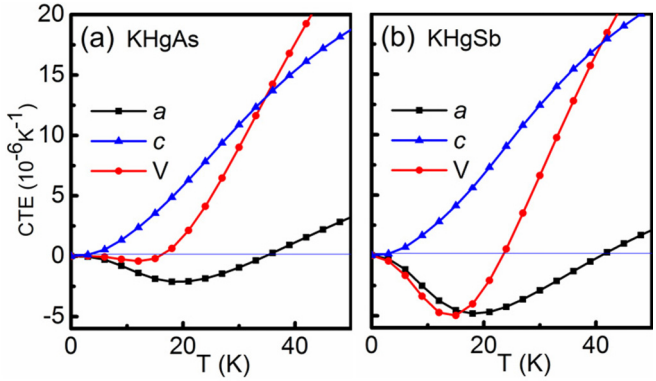

FIG. 4. Calculated CTE of (a) KHgAs and (b) KHgSb along the a and c axes and in volume.

the *ab* plane despite the presence of a PTE out of plane. It is known that, even though single-layer graphene shows larger NTE, the magnitude of the coefficient of negative thermal expansion (CNTE) of few-layer graphene decreases with the increasing number of layers [36], leading to a volumetric PTE for graphite. Since the essential unit of KHg*X* consists of alternately arranged K and Hg-*X* atomic layers, the rather soft K layer increases the distance from the Hg-*X* layer, which in turn decreases not only the interaction of adjacent Hg-*X* layers but also the magnitude of PTE in the *c* axis, thereby leading to a volumetric NTE. These abnormal thermal expansion features would be taken into account for future applications of hourglass fermion materials.

Second, the VA atoms in periodic table are found to markedly influence the NTE property. The maximal negative CTE decreases with decreasing the atomic number of *X*. We find that, when *X* is substituted by a P atom, the NTE property even disappears (see Supplemental Material Fig. S2 [35]). Therefore, KHgBi is likely to exhibit an enhanced NTE within the honeycomb plane as well as the whole volume.

Third, the alkali metal atoms also play an important role in determining the NTE property. The maximal negative CTE decreases with increasing the atomic number of alkali metal (i.e., when K is substituted by Rb, the NTE of RbHgSb is found to decrease) (see Supplemental Material Fig. S2 [35]). Thus, we can say that the lighter alkali atoms such as Li and Na may greatly enhance the NTE property of hourglass fermion materials.

Overall, the peculiar structure of the layered KHg*X* compounds results in their abnormal thermal expansion features, where both the alkali metal atoms and the VA atoms collaboratively influence the NTE property. We note that, since the presently employed PBE functional tends to overestimate the equilibrium lattice constant, our estimations for the phonon frequencies, the magnitude of the NTE, and the temperature range of the NTE could be somewhat underestimated.

C. The negative thermal expansion mechanism of KHg*X*

It is well known that thermal expansion is related to the anharmonicity of lattice vibrations. The anharmonic effects with the nonlinear vibrational degree of an atom can be reflected by the mode Grüneisen parameter. Specifically, if the excited modes with negative Grüneisen parameter (γ_i) are more dominant than those with positive γ_i, the thermal expansion becomes negative. In this sense, the Grüneisen parameter can serve as an indicator between the lattice vibrations and NTE [37]. The calculated mode Grüneisen parameters along the high-symmetry directions in BZ are illustrated in Fig. 5. It is seen that the transverse out-of-plane acoustic mode (ZA mode) at the zone center and the low-frequency optical modes [especially $B_{2g}(1)$] have large negative Grüneisen parameters, indicating that the two modes contribute dominantly to NTE.

It is noticeable that the membrane and tension effects are of importance in determining the NTE properties of two-dimensional layered materials. Figures 6(a) and 6(b) illustrate the membrane effect of the ZA mode and the tension effect of $B_{2g}(1)$ modes in KHg*X*, respectively. Since the long-range membrane effect originates from the transverse acoustic mode, the corresponding vibration of atoms form

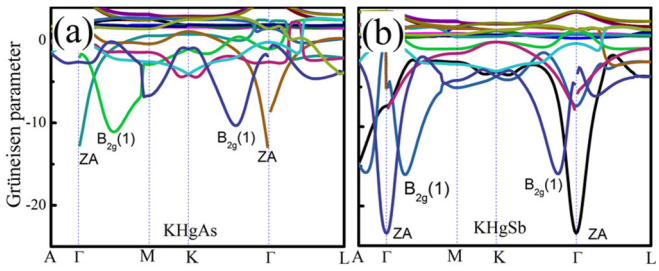

FIG. 5. Calculated mode Grüneisen parameters along the high-symmetry directions in the BZ of (a) KHgAs and (b) KHgSb.

waves or wrinkles, leading to a contraction in the layer plane accompanying an expansion in the direction perpendicular to the layer plane. Meanwhile, the short-range tension effect is caused by the low-frequency optical modes, such as the $B_{2g}(1)$ mode. Therefore, the Hg and *X* atoms vibrating perpendicular to the honeycomb layer little change the bond length of Hg-*X*, but they shorten the distance between adjacent Hg (or *X*) atoms in-plane. It is noted that the membrane effect is often seen for most layered NTE materials, while the tension effect is plausible only when the bonds are soft enough. Interestingly, the present KHg*X* systems exhibit both membrane and tension effects, thereby giving rise to a volumetric NTE.

For the layered structure, the composite elements in the planar structure are of importance in determining the NTE property. For instance, most planar layered structures, including graphite, $Ni(CN)_2$, and $CuNi(CN)_4$, have the strong C-C or C-N bonds, which can produce the NTE property mostly by the membrane effect (negligible tension effect). In this sense, such layered materials show the NTE behavior only in the layer plane, with a thermal expansion over the whole volume. By contrast, KHg*X* has the triangular K lattice as well as the honeycomb Hg-*X* layer (i.e., the Hg-*X* layer constitutes the skeleton structure with the soft K atoms spread between the Hg-*X* layers). Such a peculiar structure with the relatively weaker Hg-*X* planar bonds facilitates a large tension effect. Even though the Hg-*X* layers may have residual tensions, the resulting stress could be reconciled by the intervening K layers. This geometrical feature in KHg*X* is most likely to contribute to a significant NTE property. We note that the K layers not only enlarge the distance between adjacent honeycomb Hg-*X* layers, but also sufficiently screen the forces of the Hg-*X* layers.

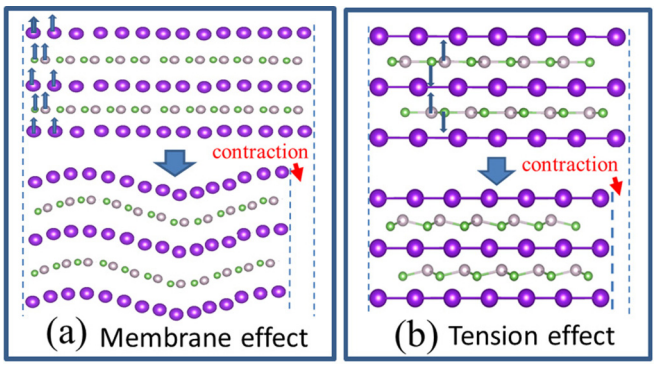

FIG. 6. Schematic diagrams of the (a) membrane and (b) tension effects for the NTE of KHg*X*.

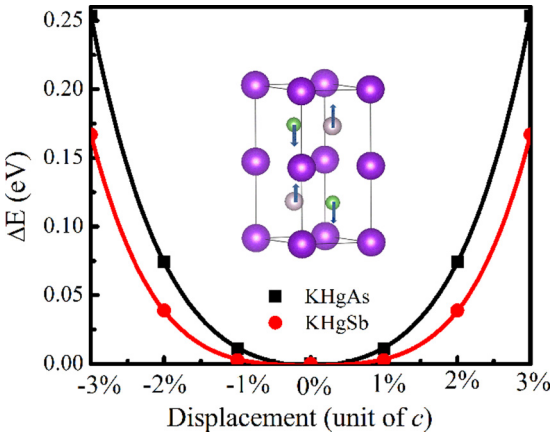

FIG. 7. Energy difference versus the displacement of the Hg and X atoms along the vibrational directions depicted in the inset.

This may result in a reduced expansion perpendicular to the layer when the honeycomb layer is contracted, leading to a volumetric NTE in KHgSb.

It is worth noting that there are the two important factors in KHgX, which facilitate not only the membrane but also tension effects: (i) the hardness of the Hg-X skeleton with a weak Hg-X bond and (ii) the motion inertia of the K layers with a light atomic mass. Due to the more electronegative and the relatively smaller size of As compared with Sb, the Hg-As bond is stronger than the Hg-Sb bond, leading to a smaller NTE in KHgAs compared with KHgSb. To examine the influence of the Hg-X skeleton on the NTE property, we also performed the calculation for the isostructural material KHgP and found that KHgP does not exhibit the NTE property due to the strong Hg-P bond, which hinders displacement of the Hg and P atoms. In this sense, it is expected that the isostructural compound KHgBi may show a lager NTE compared with KHgSb. We also examined the possible contribution to NTE from the different alkali-metal layers by calculating the NTE of RbHgSb. We found that the heavy Rb atoms suppress the vibration of HgSb perpendicular to the honeycomb layer, thus leading to much weaker NTE behavior (with a maximum negative CTE of about $-2.5 \times 10^{-6}\,\mathrm{K}^{-1}$ at 15 K along the a axis).

To provide a quantitative analysis for the tension effect, we calculate the energy barrier for the vibration of Hg and As (or Sb) atoms perpendicular to the plane. The energy barrier is calculated from the energy difference (ΔE) between the equilibrium structure and the deformed structure with the displacements of the Hg and As (or Sb) atoms along the vibration directions, as shown in Fig. 7. It is seen that the ΔE versus displacement curve of KHgAs is steeper than that of KHgSb, indicating that the vibration of the honeycomb layer is more difficult in the former than the latter. In other words, the NTE of KHgSb can be preferable compared with KHgAs, consistent with the present calculations. Of course, the quantitative evaluation for the NTE of KHgX should considered both the membrane and tension effects.

The vibration behavior of NTE materials under compression reflects the NTE property. It is known that the unusual phonon softening with decreasing volume can be associated with the observed NTE (i.e., a large phonon softening with decreasing volume corresponds to a large negative Grüneisen parameter due to $\gamma = -\frac{\partial \ln \omega}{\partial \ln V}$). Figure 8 shows the low-energy phonon frequencies of KHgAs and KHgSb at two different lattice constants a and $0.997a$. We find that, as volume decreases, the high-frequency phonon modes show a hardening behavior, whereas the acoustic and lower optical phonon modes have a softening behavior. The phonon softening is more dominant in KHgSb than KHgAs, indicating a larger NTE in KHgSb. The softening of phonon modes around the Γ (0, 0, 0) point may represent a greater anharmonicity, which in turn contributes to NTE. Obviously, this is consistent with the negative Grüneisen parameter, as shown in Fig. 5. We also find that, as the lattice constant a decreases by 1.2%, the lowest optical phonon mode Γ_1 [shown in Fig. 8(b)] at the Γ point begins to show imaginary frequency, indicating that the compression up to some degree would give rise to the phase transition of KHgSb, as previously reported in ReO_3 [38]. We believe that, although the minimal imaginary modes can slightly reduce the thermodynamic free energy, the NTE behavior predicted in KHgX would be unlikely to change.

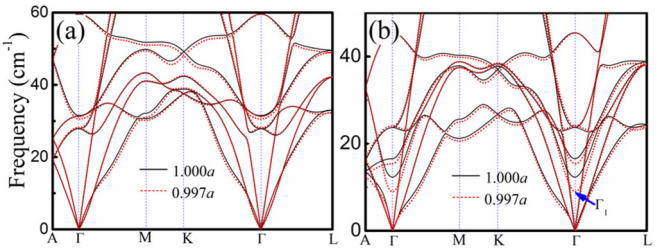

FIG. 8. Low-energy phonon frequencies of (a) KHgAs and (b) KHgSb at two different lattice constants, a and $0.997a$.

IV. SUMMARY

We investigated the vibrational and NTE properties of the "hourglass fermion" materials KHgX (X = As, Sb) using first principles DFT calculations combined with the quasi-harmonic approximation. We found that these layered materials exhibit an abnormal volumetric thermal expansion due to their peculiar structures, which can be regarded as a NTE material. Our analyses of the Grüneisen parameters and vibrational modes revealed that the NTE of KHgX is driven by cooperation of the membrane and tension effects. Furthermore, we demonstrated that the weaker bonds in Hg-X and the smaller mass of the alkali metal will facilitate the membrane and tension effects, thereby giving rise to an NTE property. Our results not only provide insights for understanding the underlying mechanism involved in the NTE properties of two-dimensional layered KHgX materials but also open an exciting direction for future experimental and theoretical research on the thermal effects of hourglass fermions.

ACKNOWLEDGMENTS

C.-Y.N and Y.J thank the support by the National Natural Science Foundation of China (Grants No. 11504332 and No. 11274280); J.-H.C. acknowledges support by the National Research Foundation of Korea (NRF) grant funded by the Korea Government (MSIP) (No. 2015R1A2A2A01003248).

[1] H. Weng, X. Dai, and Z. Fang, MRS Bull. **39**, 849 (2014).
[2] M. Wada, S. Murakami, F. Freimuth, and G. Bihlmayer, Phys. Rev. B **83**, 121310 (2011).
[3] Z. K. Liu, J. Jiang, B. Zhou, Z. J. Wang, Y. Zhang, H. M. Weng, D. Prabhakaran, S. K. Mo, H. Peng, P. Dudin, T. Kim, M. Hoesch, Z. Fang, X. Dai, Z. X. Shen, D. L. Feng, Z. Hussain, and Y. L. Chen, Nat. Mater. **13**, 677 (2014).
[4] R. Yu, H. Weng, Z. Fang, X. Dai, and X. Hu, Phys. Rev. Lett. **115**, 036807 (2015).
[5] S.-M. Huang, S.-Y. Xu, I. Belopolski, C.-C. Lee, G. Chang, B. Wang, N. Alidoust, G. Bian, M. Neupane, C. Zhang, S. Jia, A. Bansil, H. Lin, and M. Z. Hasan, Nat. Commun. **6**, 7373 (2015).
[6] H. Weng, C. Fang, Z. Fang, B. A. Bernevig, and X. Dai, Phys. Rev. X **5**, 011029 (2015).
[7] Z. Wang, A. Alexandradinata, R. J. Cava, and B. A. Bernevig, Nature **532**, 189 (2016).
[8] A. Alexandradinata, Z. Wang, and B. A. Bernevig, Phys. Rev. X **6**, 021008 (2016).
[9] J.-Z. Ma, C.-J. Yi, B. Q. Lv, Z. J. Wang, S.-M. Nie, L. Wang, L.-Y. Kong, Y.-B. Huang, P. Richard, H.-M. Weng, B. A. Bernevig, Y.-G. Shi, T. Qian, and H. Ding, arXiv:1605.06824.
[10] C. Lind, Materials **5**, 1125 (2012).
[11] T. A. Mary, J. S. O. Evans, T. Vogt, and A. W. Sleight, Science **272**, 90 (1996).
[12] A. Sanson, F. Rocca, G. Dalba, P. Fornasini, R. Grisenti, M. Dapiaggi, and G. Artioli, Phys. Rev. B **73**, 214305 (2006).
[13] X. Wang, Q. Huang, J. Deng, R. Yu, J. Chen, and X. Xing, Inorg. Chem. **50**, 2685 (2011).
[14] R. Mittal and S. L. Chaplot, Phys. Rev. B **78**, 174303 (2008).
[15] K. Nakano, K. Oka, T. Watanuki, M. Mizumaki, A. Machida, A. Agui, H. Kim, J. Komiyama, T. Mizokawa, T. Nishikubo, Y. Hattori, S. Ueda, Y. Sakai, and M. Azuma, Chem. Mater. **28**, 6062 (2016).
[16] K. Takenaka and H. Takagi, Appl. Phys. Lett. **87**, 261902 (2005).
[17] T. Hamada and K. Takenaka, J. Appl. Phys. **109**, 07E309 (2011).
[18] B. K. Greve, K. L. Martin, P. L. Lee, P. J. Chupas, K. W. Chapman, and A. P. Wilkinson, J. Am. Chem. Soc. **132**, 15496 (2010).
[19] K. W. Chapman, P. J. Chupas, and C. J. Kepert, J. Am. Chem. Soc. **127**, 15630 (2005).
[20] J. C. Hancock, K. W. Chapman, G. J. Halder, C. R. Morelock, B. S. Kaplan, L. C. Gallington, A. Bongiorno, C. Han, S. Zhou, and A. P. Wilkinson, Chem. Mater. **27**, 3912 (2015).
[21] N. Mounet and N. Marzari, Phys. Rev. B **71**, 205214 (2005).
[22] R. Mittal, M. Zbiri, H. Schober, E. Marelli, S. J. Hibble, A. M. Chippindale, and S. L. Chaplot, Phys. Rev. B **83**, 024301 (2011).
[23] A. M. Chippindale, S. J. Hibble, E. Marelli, E. J. Bilbe, A. C. Hannon, and M. Zbiri, Dalton Trans. **44**, 12502 (2015).
[24] I. M. Lifshitz, Zh. Eksp. Teor. Fiz. **22**, 475 (1952).
[25] G. Kresse and J. Furthmüller, Phys. Rev. B **54**, 11169 (1996).
[26] G. Kresse and D. Joubert, Phys. Rev. B **59**, 1758 (1999).
[27] J. P. Perdew, K. Burke, and M. Ernzerhof, Phys. Rev. Lett. **77**, 3865 (1996).
[28] A. Togo, F. Oba, and I. Tanaka, Phys. Rev. B **78**, 134106 (2008).
[29] P. Souvatzis and O. Eriksson, Phys. Rev. B **77**, 024110 (2008).
[30] F. D. Murnaghan, Proc. Natl. Acad. Sci. USA **30**, 244 (1944).
[31] R. Mittal, S. L. Chaplot, S. K. Mishra, and P. P. Bose, Phys. Rev. B **75**, 174303 (2007).
[32] R. Vogel and H.-U. Schuster, Z. Naturforsch. B **35**, 114 (1980).
[33] J. M. Skelton, D. Tiana, S. C. Parker, A. Togo, I. Tanaka, and A. Walsh, J. Chem. Phys. **143**, 064710 (2015).
[34] H. M. Tütüncü and G. P. Srivastava, Philos. Mag. **94**, 2692 (2014).
[35] See Supplemental Material at http://link.aps.org/supplemental/10.1103/PhysRevB.95.104101 for supplementary Figs. S1 and S2 and Tables S1 and S2.
[36] K. V. Zakharchenko, J. H. Los, M. I. Katsnelson, and A. Fasolino, Phys. Rev. B **81**, 235439 (2010).
[37] Z. Wang, F. Wang, L. Wang, Y. Jia, and Q. Sun, J. Appl. Phys. **114**, 063508 (2013).
[38] T. Chatterji, P. G. Freeman, M. Jimenez-Ruiz, R. Mittal, and S. L. Chaplot, Phys. Rev. B **79**, 184302 (2009).